Mode selectivity of SH guided waves by dual excitation and reception applied to mode conversion analysis

Alan C. Kubrusly, Miguel A. Freitas, Jean Pierre von der Weid and Steve Dixon

***Abstract*—SH guided waves, generated by periodic permanent magnet arrays have been used previously in non-destructive evaluation of metal plates and pipes. When an SH guided wave interacts with a defect or change in sample thickness, the incident SH wave may undergo mode conversion. Analysis of mode conversion is complicated, due to the interference of several propagating modes in the received signal, that can often temporally overlap. This paper proposes a mode selection technique to help understand the interaction of SH guided waves with changes in sample thickness. Using an understanding of the propagation characteristics of the guided waves, SH guided waves are sequentially generated and detected on both surfaces of the plate, capturing four distinct waveforms. By superposition of the detected signals, symmetric modes can be clearly separated from antisymmetric modes in the processed, received signals. For this method to work well, the transducers used should have very similar responses and be precisely positioned on exactly opposite positions either side of the plate. Finite element simulations are also performed, mirroring the experimental measurements, and the results correlate well with the experimental observations made on an 8 mm thick plate with a region of simulated wall thinning machined into the sample.**

***Index Terms*—SH guided waves, mode conversion, mode selection, PPM EMAT, superposition principle.**

I. Introduction

The use of Shear Horizontally (SH) polarised waves generated and detected by Electromagnetic Acoustic Transducer (EMAT), especially Periodic Permanent Magnet (PPM) EMAT [1]–[4], is of industrial interest, as the waves have a number of interesting properties for NDT applications and can be generated and detected without contact. SH guided waves can propagate in plates, or circumferentially around pipes as a slightly different class of SH guided wave [5]–[7]. When an SH guided wave is incident upon a thinner thickness region, such as a corrosion like defect, mode conversion can occur in reflection and transmission whenever the dispersion curve allows it [6], [7]. The SH guided wave interaction and mode conversion phenomenon with wall thinning type defects is not yet completely understood, and an understanding is required to establish a reliable inspection procedure. Preliminary research [6]–[9] has investigated the problem of SH guided wave interaction with a machined region designed to crudely simulate a corrosion like defect. Previous researchers observed that mode conversion depends on the profile of the edge from the thick to the thinner region of the plate [9], but no quantitative analysis has been undertaken. The interference of several mode-converted waves can lead to signals that are difficult to interpret, which usually only allows qualitative analysis.

In order to quantitatively assess mode conversion, one has to be able to generate a single mode and then separate the many possible modes present in the received signal: if a single symmetric mode is excited, then both symmetric and antisymmetric modes can be generated in regions of plate thinning by mode conversion [8], [9]. Modes with different group velocities will eventually temporally separate, but the distance required for this may be prohibitively large if the group velocity of the modes are close, or if long pulses are used for excitation [10]. More importantly, if the position in which mode conversion has taken place is unknown, this approach is very limited, as the propagating path is unpredictable.

There are several signal processing techniques for mode separation or identification by comparison with the theoretical dispersion cures, some of which obtain mode dispersion characteristics using a 2D Fourier transform [11], [12] or some time-frequency representation [13]–[15]. Some of these methods require several detection points, and signal reconstruction in the time domain may be not straightforward. Other approaches use a priori knowledge of the ultrasonic propagation path and the theoretical dispersion curve to compensate for dispersion of a wideband pulse, to identify a particular guided wave mode [16], [17].

A single mode of interest can be generated by enhancing its excitability when compared to other modes. This can be performed by either imposing the stress profile or the wavelength in which one specific mode of interest presents higher responsiveness than the others. Schmidt et al. [18], [19] analytically designed and experimentally evaluated an interdigital piezocomposite transducer in which the distance between elements was set to match the A0 Lamb wave wavelength, highly increasing this mode amplitude compared to the others. Koduro and Rose [20] used an interdigital annular transducer for selecting the S1 or A1 Lamb modes in an omnidirectional guided wave tomographic system to experimentally detect corrosion defects. Recently Moghadam et al. analytically [21] and experimentally [22] evaluated an algorithm to optimise the shear stress profile in order to determine the optimal transducer size and number of elements of a multi-element piezoelectric actuator for mode selectivity excitation.

A. C. Kubrusly, M. A. Freitas and J. P non der Weid are with the Centre for Telecommunication Studies, Pontifical Catholic University of Rio de Janeiro, Rio de Janeiro, Brazil e-mail: alan@cetuc.puc-rio.br

S. Dixon is with Department of Physics, University of Warwick, Coventry, England, UK

Symmetric modes present the tangential component of the displacement on both surfaces in phase, whereas antisymmetric modes have out of phase tangential displacement. Based on this characteristic, selection of either symmetric or antisymmetric modes can be achieved by simultaneously exciting transducers on opposite faces of the waveguide, in phase or out of phase. Su and Ye [23] used this principle in a composite plate in which the connection of piezoelectric transducers was controlled by an electric circuit in order to enhance or suppress the fundamental symmetric or antisymmetric Lamb wave modes. The same technique was later used, also with Lamb waves, by Kim et al. [24] on aluminium plates with distributed sensors and by Shelke et al. [25] for detection of delamination in laminated aluminium plate. The technique can be used also with EMAT transmitters. Recently, Liu et al. [26] evaluated through numerical simulations the use of two Lamb wave EMATs in order to selectively generate either only the A0 or S0 Lamb wave modes. Analogously, a dual receiver was used by Schmidt et al. [18] in order to verify the efficacy of mode selectivity on transmission by an interdigital transducer. There is however little published research on simultaneous dual generation and reception.

With PPM EMAT both frequency and wavelength can be selected. However, in practice, this selection relies on a finite locus in the dispersion curves [6], [27]. If the dispersion curve of more than one mode lies in this locus, then mode selection is compromised, because more than one mode is excitable. If one can have access to both sides of the waveguide, then dual transduction can be used together with wavelength and frequency bandwidth tuning in order to improve control over the selection of guided wave mode generation. In this paper, a combination of dual transmission and dual reception of SH guided waves with PPM EMATs is investigated as a technique for mode selection of either converted or non-converted modes. The proposed methodology can be used as an experimental instrument for quantitative investigation of mode conversion in a controlled framework, where one can have access to both sides of a plate. The technique's experimental limitations are assessed, and it is then validated for mode conversion analysis of SH guided waves interacting with a machined region simulating a wall thinning defect.

II. SH GUIDED WAVE THEORY

SH guided waves present the particle vibration in-plane, being parallel to the surface of the material and perpendicular to the propagation direction [28]. Considering that x is the propagation direction, y is the coordinate of the plate thickness, z is the polarisation direction, the non-zero displacement component of an SH guided wave mode on a plate is given by

$$u_z(x,y,t) = A_n U_n(y) e^{j(\kappa x - \omega t)} \quad , \tag{1}$$

where κ the angular wavenumber, ω the angular frequency, n is the mode order index, A_n is the amplitude of each mode and $U_n(y)$ is the displacement profile along the y coordinate for each mode. Fig.1 illustrates the coordinate system and the SH wave displacement polarisation.

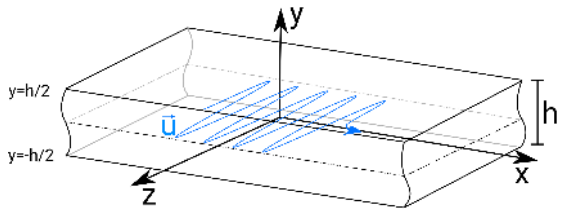

Fig. 1. Coordinate system and SH guided wave polarisation and propagation direction in a plate with thickness h.

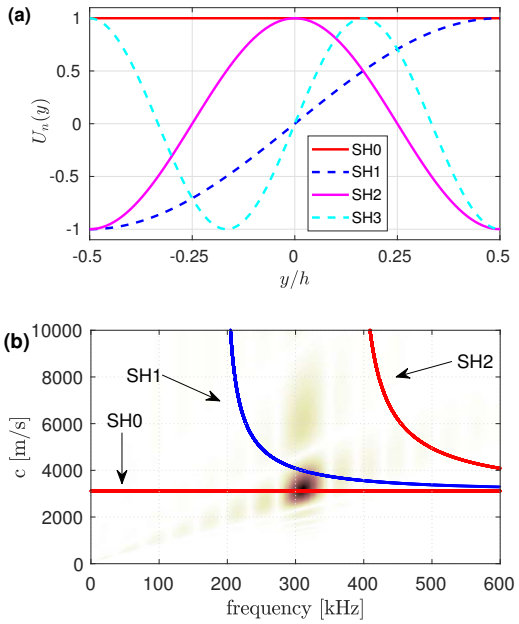

Fig. 2. (a) SH modes displacement profile, continuous lines are for symmetric modes whereas dashed lines are for antisymmetric modes. (b) Phase velocity dispersion curves for an 8 mm aluminium plate superposed to the operating region, colour plot, for a 3 cycle PPM EMAT with 10mm spatial period excited with 8 cycle current tone burst at 311kHz for SH0 excitation, the darker the colour the higher the excitability.

SH guides waves can be either symmetric or antisymmetric. This classification is related to the variation of the z component of the displacement field along the y axis. Even order modes (n even) are symmetric whereas odd order modes (n odd) are antisymmetric. The displacement profile for symmetric and antisymmetric SH modes on a plate with thickness h is given, respectively, by (2a) and (2b)

$$U_n(y) = \begin{cases} cos(n\pi y/h), & n = \{0,2,4,...\} \quad (2a) \\ sin(n\pi y/h), & n = \{1,3,5,...\} \quad (2b) \end{cases}$$

Fig. 2(a) shows the displacement profile for modes SH0, SH1, SH2 and SH3, corresponding to orders n = 0 to 3, respectively; SH0 and SH2 are symmetric and SH1 and SH3 are antisymmetric.

SH guided waves are generally dispersive, meaning that the phase and group velocities are frequency dependent. This dependence is given by (3a) and (3b) for phase and group

velocities, respectively

$$c = c_T \, 2fh \Big/ \sqrt{4(fh)^2 - n^2 c_T^2} \quad , \tag{3a}$$

$$c_g = c_T \sqrt{1 - \left(nc_T/2fh\right)^2} \quad , \tag{3b}$$

where c_T is the transverse wave speed of the material, and f is the frequency [28]. Fig. 2(b) shows the phase velocity dispersion curves for modes SH0 to SH2 for an 8 mm thick aluminium plate. Uniquely for the fundamental SH0 mode, there is no dispersion and phase and group velocities are constantly equal to c_T. All dispersive SH guided wave modes have real solutions for phase and group velocity from a determined frequency×thickness (fh) value, say $(fh)_{\text{cut-off}}$ given by

$$(fh)_{\text{cut-off}} = nc_T/2 \quad , \tag{4}$$

which means that propagating modes only occur if the operating fh is above this value. Alternatively, for a fixed frequency, the modes only exist if the plate thickness is above the cut-off thickness, given by

$$h_{\text{cut-off}} = nc_T/2f \quad . \tag{5}$$

SH guided waves present some advantages over Lamb waves [28], such as: (i) shear-horizontal vibrations propagate without coupling to longitudinal waves, (ii) their properties only depend on c_T and plate thickness, (iii) they have a much simpler displacement profile, (iv) have much simpler dispersion curves, (v) have a simpler relationship for the cut-off frequency and (vi) no energy leakage to a non-viscous fluid in contact with the plate. However, SH waves can be difficult to generate, compared to other wave modes.

III. Periodic Permanent Magnet Electromagnetic Acoustic Transducer

SH waves can be generated by a PPM EMAT, which consists of an array of magnets with alternate polarity and an elongated spiral or racetrack coil. In aluminium, EMATs induce Lorentz force, given by

$$\mathbf{F} = \mathbf{J} \times \mathbf{B} \tag{6}$$

where $\mathbf{B}$ is the magnets static magnetic field and $\mathbf{J}$ is the electric current density induced in the sample, which is opposite to the current flowing in the coil (I); the symbol $\times$ means the cross product between two vectors [1]. In a PPM EMAT, magnet array and coil are positioned in such a way that the alternating induced forces in the sample lie along the z direction, generating a z-polarised shear wave that propagates perpendicularly to the forces, i.e., along the x axis, as schematically shown Fig. 3, in which two PPM arrays and coils are placed over and underneath a sample.

The induced forces distribution in the material can be approximated by a spatial tone-burst according to the magnets periodicity and number of elements on the array [27]. Therefore, a spatial spectrum is defined by its Fourier Transform, which corresponds to the excitability as a function of the wavenumber. The limited number of spatial cycles leads to a finite spatial bandwidth. Similarly, the time-dependent

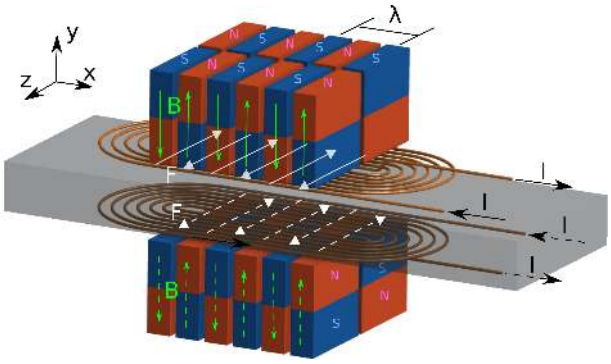

Fig. 3. Two identical PPM EMAT positioned on both surfaces of the plate. Blue and red blocks represent the magnets south (S) and north (N) pole, respectively. The coil is positioned underneath the magnets, between them and the test sample. Arrows represent the coil current (I), static magnetic field (B) and generated Lorentz force (F). All entities related to the lower transducer are represented by dashed arrows. The spacing between magnets imposes the central wavelength (λ).

excitation current in the coil produces a frequency bandwidth. The intersection of spatial and temporal bandwidths produces a locus in the wavenumber-frequency plane of excitable waves; this is the transducer operating region. Using the relationship $c = \omega/\kappa$, one can translate the operating region to the phase velocity - frequency plane. Fig. 2(b) shows the operating region for a 3 cycle PPM EMAT with 10 mm spatial period driven by a current 8 cycle tone burst at 311 kHz superposed to the phase velocity dispersion curve of an 8 mm thick aluminium plate. It is noticeable that the SH0 dispersion curve crosses the centre of the operating region, therefore it is predominately generated, but the SH1 is also generated with non-negligible intensity.

The same principle applies for receiving an SH guided wave by a PPM EMAT, such that if the EMAT used to detect an SH wave whose wavelength and frequency lie outside the transducer's operating region, then no signal is detected. Strictly speaking, as the operating region presents a smooth decay, any shift on wavelength and frequency would lead to attenuation in the detected signal.

IV. Mode selectivity

Mode selectivity can be obtained by narrowing both frequency and spatial bandwidths and by generating symmetric or antisymmetric modes, as shown schematically in Fig. 4. In this example, a three cycle force is applied simultaneously in both surfaces at the same longitudinal position. Placing two identical transducers at the same longitudinal position on opposite sides of the plate's surfaces and triggering them simultaneously (dual excitation) in-phase or out-of-phase, has been previously employed for Lamb waves [23]–[25]. When using this technique to analyse mode conversion arising due to wave's interaction with some feature in the plate for instance, more than one mode can be received at a third detection transducer, but the sensitivity to the mode converted wave will depend on its wavelength and the spatial impulse response of the receiver. Mode selectivity can also be implemented in reception if detection is performed on both sides of the plate

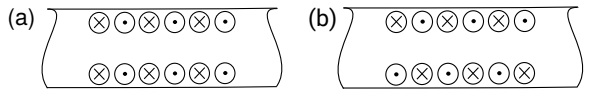

Fig. 4. Symmetric (a) and antisymmetric (b) generation, the symbols ⊙ and ⊗ stands for applied forces oriented outward and inward the paper sheet, respectively.

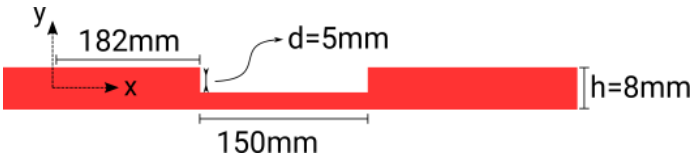

Fig. 5. Plate and defect geometry.

at the same longitudinal position. By properly combining the signals received at the top ($y = h/2$) and bottom ($y = -h/2$) surfaces of plate, at the same longitudinal position, one can separate the symmetric and antisymmetric parts of the detected displacement field. The symmetric and antisymmetric parts are defined by (7).

$$u_S = (u_T + u_B)/2 \quad , \tag{7a}$$

$$u_A = (u_T - u_B)/2 \quad , \tag{7b}$$

where u is the signal of interest, the subscripts S and A are for the symmetric and antisymmetric parts respectively, and the subscripts T and B are for the top and bottom surfaces, respectively. The symmetric component, (7a), is composed only of symmetric modes since the antisymmetric modes are nullified by summing the signal on both surfaces, as they present opposite signs at the surfaces. Conversely, the antisymmetric component, (7b), contains only antisymmetric modes. Combining the method for selectivity of antisymmetric or symmetric modes for generation and detection allows one to thoroughly investigate mode conversion from a single mode, seeing how it could generate symmetric and antisymmetric components.

V. Numerical Implementation of Mode Selectivity

In order to verify the capability of the mode selectivity technique, finite element analysis was performed in an 8 mm aluminium plate model with a region that has been machined thinner. For numerical analysis: A commercial, time-domain, Finite Element Method (FEM) solver, PZFlex© was used, which allows simulation of SH waves in a two-dimensional model, in this paper. The material has been modelled with density ρ=2698 kg/m^3 and transverse wave speed c_T=3111 m/s. The geometry is shown in Fig. 5, in which the plate's plane lies in the x-y plane (thickness in the y direction, length in the x direction). Both ends of the plate are terminated with absorbing boundary condition, to try to simulate an infinite medium. A defect is modelled as a stepped thickness reduction beginning at 182 mm with total length of 150 mm, thus finishing at 332 mm, and depth of 5 mm. A mesh with 50 elements per wavelength was used after convergence test has confirmed its sufficiency by comparing the results with incremental numbers of elements per wavelength.

In order to simulate PPM EMAT transduction in the model, forces along the z direction were directly applied to the surfaces nodes in such a way to imitate the PPM EMAT induced forces. For this, the applied force distribution followed a spatial tone burst centred at the origin, either on the top or the bottom surface, as described by (8):

$$f_{T,B}[i] = C_{T,B}\, sin(2\pi x[i]/\lambda),\ -N\lambda/2 \leq x[i] \leq N\lambda/2\,, \tag{8}$$

where, $f_{T,B}[i]$ is the applied force at node i, at the top (T) or bottom (B) surfaces, $C_{T,B}$ is the respective amplitude, $x[i]$ is the x position of node i, λ and N are the centre wavelength and the number of spatial period of the PPM array, respectively. Here, N = 3, and $\lambda = 10mm$. Since force was not applied to a single point, but instead followed (8), then the spatial distribution of the PPM EMAT induced forces are approximately simulated, as similarly performed and validated in [10], [29], without the need of including the whole EMATs into the model.

Dual excitation was employed in the simulation following the procedure of section IV. Symmetric modes were generated by setting $C_T = C_B = 1$, whereas antisymmetric modes by setting $C_T = 1$ and $C_B = -1$ as shown in Fig. 4(a) and (b), respectively. The forces were varied in time as an 8 cycle tone-burst at 311 kHz or 367 kHz, in order to generate the symmetric SH0 mode or antisymmetric SH1 mode, respectively. The corresponding minimum thicknesses that can support the SH1 mode propagating, according to (5), are 5.0 mm and 4.2 mm for frequencies of 311 kHz and 367 kHz respectively, so that no SH1 mode is expected to propagate inside the thinner region of the plate.

Fig. 6(a) shows the particle velocity on the top surface of the plate for generating only the SH0 mode, for increasing time. The colour scale represents the magnitude of the velocity. Wave generation occurs at the origin; the wave front propagating to the left (negative direction) is absorbed by the absorbing boundary condition. At the start of the thinner region reflections occur; with the reflected wave propagating towards the negative x direction. The reflected wave shows interference effects in amplitude or beating [10], pulse widening or dispersion, suggesting the presence of more than one mode, due to mode conversion of the SH0 to the SH1 mode. On the defect area, the original SH0 mode is dominant as would be expected below cut off for higher order modes. At the end of the defect, the mode beating pattern is seen again, suggesting the presence of more than one mode from mode conversion.

The use of dual excitation ensures single mode generation, as shown in Fig. 6(a). However, where mode conversion occurs, it is not always possible to separately observe the modes in the time domain looking at the displacement at one surface, making any quantitative analysis difficult. Dual reception is further applied, Fig. 6(b) and (c) show the symmetric and antisymmetric fields, obtained by applying the top and bottom fields into (7a) and (7b), respectively, allowing us to observe symmetric and antisymmetric modes separately. The symmetric field clearly shows a weak SH0 reflection at the defect, and strong transmission into the defect, followed by low transmission out of the defect. The antisymmetric component shows the SH1 reflected at the defect and transmitted

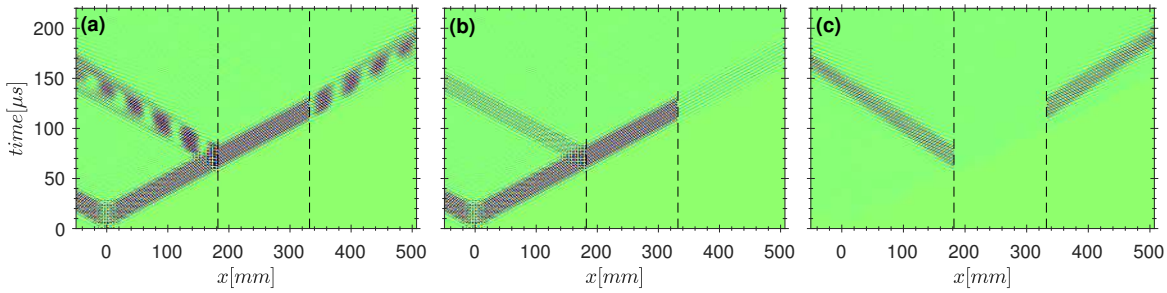

Fig. 6. Numerical simulation of SH0 mode generated in a plate with defect. (a) Top surface, (b) symmetric part, and (c) antisymmetric part. Dashed lines represent the edges of the thinner region.

out of the far end of the defect due to mode conversion. No antisymmetric component is found inside the defect, as expected.

Similar analysis was done, generating an SH1 mode, using antisymmetric excitation at 367 kHz and is shown in Fig. 7(a). The symmetric and antisymmetric mode selectivity by dual reception is shown in Fig. 7(b) and (c), respectively. Reflection at the defect and transmission out of the far end of the defect of both symmetric and antisymmetric modes occur. On the defect, it was confirmed that there is no antisymmetric oscillation, so that the SH1 mode transmitted away from the defect right end must be due to mode conversion from the SH0 to the SH1 mode at the step up in thickness. Dual reception allows one to test the effectiveness of dual generation. In both cases the absence of the opposite polarisation (symmetric or antisymmetric) around the origin confirms that the polarisation of interest is only being generated.

VI. Experimental validation

In order to perform dual generation on both surfaces of the plate experimentally, as illustrated in Fig. 4(a) and (b) one has to be able to simultaneously and equally excite two transducers positioned on the two plate's surfaces. One could use two EMATs on each side of the plate, electrically connecting the EMATs in series, with one current pulser driving current either the same way or in opposite directions in each coil as drivers. Dual reception could be implemented by connecting two EMATs in series to one amplifier, or separately to two different amplifiers as receivers. In the case where two EMATs receiver amplifiers are used the signals have to be summed or subtracted to obtain the antisymmetric or symmetric mode signals.

Unfortunately real EMATs are often slightly different in performance, which generally is not significant, but for the technique described in this paper to work, they really need to be very similar. If the EMATs are not identical, and are not positioned exactly opposite each other, the excitation or detection in both surfaces would not produce a pure symmetric or antisymmetric mode. It is worth noticing that when two identical PPM EMAT transducers are positioned on both surfaces of the plate, there is an inherent phase inversion on the generated field in the material. This happens because the transducer has to be flipped down to be placed at the bottom surface, and thus the relative position between magnets and coil direction are inverted. Fig. 3 illustrates how the induced forces on the material are opposed when the electric current in the coils has the same direction (series connection).

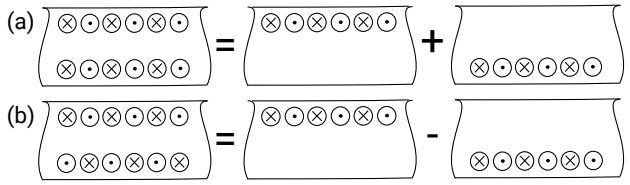

Fig. 8. Symmetric (a) and antisymmetric (b) generation or reception by using the principle of superposition.

A. Transducers similarity and the superposition principle

As stated already, due to the many components within an SH EMAT, it is very difficult to make two EMATs with identical performance. This is an issue when two could be used simultaneously on either side of a plate to generate or detect either purely symmetric or purely antisymmetric SH wave modes. This issue has been overcome by using the same transducer to generate the SH guided waves on each side of the plate, separately, whilst another EMAT is used as a receiver to detect the waves on each side of the plate separately. The generation EMAT is used on one side of the plate, whilst detecting two separate waveforms with the detector first on one side of the plate and then on exactly the opposite side of the plate. The generation EMAT is then moved to exactly the opposite side of the plate, and two detected waveforms are recorded using a separate EMAT as described previously. In this way, the four waveforms can be combined using superposition to experimentally show what purely symmetric or antisymmetric modes are present due to symmetric and antisymmetric generation and reception, allowing for quantitative analysis when only the SH0 and SH1 wave modes are present. The superposition approach is shown schematically in Fig. 8 for either generation or reception.

Reception on the top and bottom surfaces due to a symmetric and antisymmetric generation by superposition are given

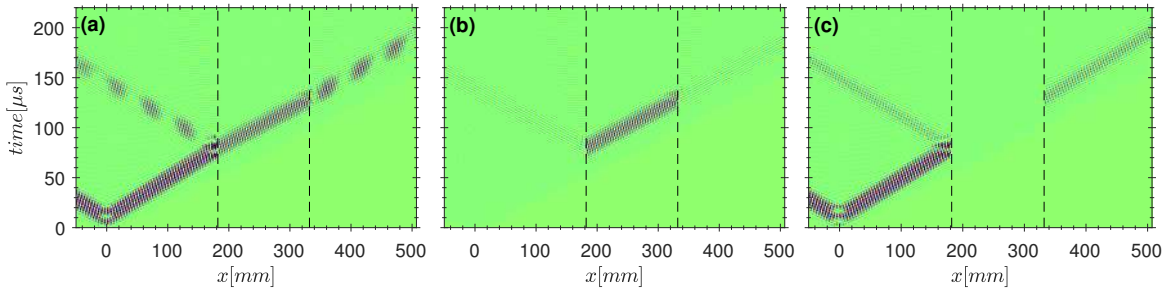

Fig. 7. Numerical simulation of SH1 mode generated in a plate with defect. (a) Top surface, (b) symmetric part, and (c) antisymmetric part. Dashed lines represent the edges of the thinner region.

respectively by

$$u_T\big|_S = \left(u_T\big|_T + u_T\big|_B\right)/2 \quad , \tag{9a}$$
$$u_B\big|_S = \left(u_B\big|_T + u_B\big|_B\right)/2 \quad , \tag{9b}$$
$$u_T\big|_A = \left(u_T\big|_T - u_T\big|_B\right)/2 \quad , \tag{9c}$$
$$u_B\big|_A = \left(u_B\big|_T - u_B\big|_B\right)/2 \quad , \tag{9d}$$

where the subscript after the vertical bar indicates how generation has been done.

Consequently, applying (9) into (7), all the possible combinations of symmetric and antisymmetric reception due to a symmetric and antisymmetric generation are given by

$$u_S\big|_S = \left(u_T\big|_T + u_T\big|_B + u_B\big|_T + u_B\big|_B\right)/4 \quad , \tag{10a}$$
$$u_A\big|_S = \left(u_T\big|_T + u_T\big|_B - u_B\big|_T - u_B\big|_B\right)/4 \quad , \tag{10b}$$
$$u_S\big|_A = \left(u_T\big|_T - u_T\big|_B + u_B\big|_T - u_B\big|_B\right)/4 \quad , \tag{10c}$$
$$u_A\big|_A = \left(u_T\big|_T - u_T\big|_B - u_B\big|_T + u_B\big|_B\right)/4 \quad . \tag{10d}$$

Recall that due to the field inversion on the bottom transducer, relative to the top one, highlighted above, all the electric signals acquired from the bottom transducer should be multiplied by -1 prior to calculating (10). It is also worth noting, when flipping an EMAT from one surface to another, if there are small differences in the lateral position and alignment of the EMAT on one side and then on the other, the superposition principle approach will be compromised.

B. Transducer alignment and mismatch error

In order to understand how misalignment can introduce errors on the mode selection procedure, one can use the most general case of a continuous sine wave signal. Let Δx be the longitudinal misalignment between both surfaces. This is related to the error in phase by $\Delta\phi = 2\pi\Delta x/\lambda$. Considering the case of symmetric continuous sine wave propagating in a defect-free plate, in which the bottom receiver presents a phase error due to misalignment. The antisymmetric field, given by (7b), becomes

$$\begin{aligned} u_{opp} &= [sin(2\pi f) - sin(2\pi f + \Delta\phi)]/2 \\ &= sin\left(\Delta\phi/2\right) cos\left(2\pi f + \Delta\phi/2\right) \quad , \end{aligned} \tag{11}$$

where the subscript "*opp*" means that this field represent the selection of the opposite mode, in this case the antisymmetric mode. The amplitude error is

$$\mathcal{E}_{opp} = sin\left(\pi\Delta x/\lambda\right) \approx \pi\Delta x/\lambda \quad , \tag{12}$$

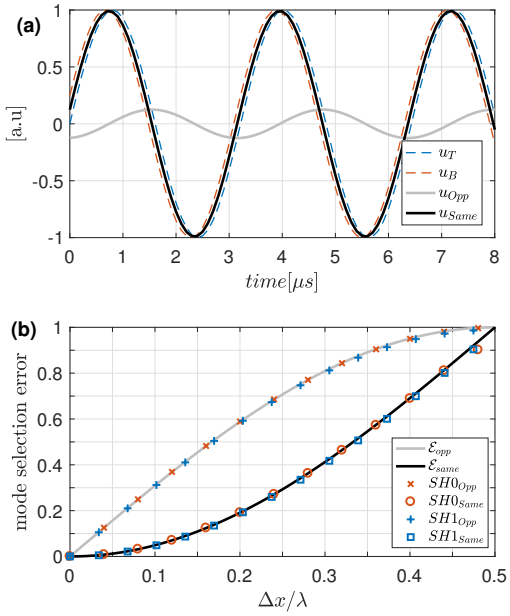

Fig. 9. Misalignment effect on mode selection. Sine wave example with 0.4 mm misalignment (a). Mode selection error versus positioning error (b), theoretical (lines) and numerical (markers) values.

where the approximation holds for small phase errors. Fig. 9(a) illustrates the case for a symmetric, continuous sine wave at f = 311 kHz and λ = 10 mm, in which there is a positioning error of 0.4 mm between the top and bottom receivers; despite this small misalignment, the amplitude of u_{opp} (grey line) is significant. Fig. 9(b) shows the error on the opposite mode signal (grey line), versus the positioning error.

The same analysis can be done for the error on the selection of same mode signal, from (7a), leading to

$$u_{same} = cos\left(\Delta\phi/2\right) sin\left(2\pi f + \Delta\phi/2\right) \quad , \tag{13}$$

the amplitude error is thus

$$\mathcal{E}_{same} = 1 - cos\left(\pi\Delta x/\lambda\right) \approx \left(\pi\Delta x/\lambda\right)^2/2 \quad . \tag{14}$$

In this case when no mode conversion occurs, the cosine that modulates u_{same} should be identically unity when there is no misalignment; consequently, $\mathcal{E}_{same}$ should be null. Comparing (14) and (12), one may see that

$$\mathcal{E}_{same} \approx \mathcal{E}_{opp}^2/2 < \mathcal{E}_{opp} \quad , \tag{15}$$

indicating that misalignment is more severe on selecting the opposite mode.

This case is also illustrated in Fig. 9(a): u_{same} (black line) is almost superposed on the top and bottom signals (dashed lines). The error calculated in (14) is plotted in Fig. 9(b) (black line), showing that for small misalignments, the error on selecting the same polarisation is much lower than for the opposite polarisation.

Without loss of generality, this example is valid for the case of continuous antisymmetric sine waves, where one should use (7a) to calculate the opposite field. However, the signal from the bottom position is 180° out of phase, compared to the top signal, resulting in the same expressions given by (11). The same reasoning holds for (13).

Mode selectivity assessment was also done for a more realistic tone burst wave, giving the same result as the sine wave. Numerical simulation was used with the same parameters as in section V, but in a non defective plate. The SH0 and SH1 modes were generated and received at 405mm. Fig. 9(b) shows the error on the same and opposite polarisation selection for the SH0 and SH1 generated modes. As it can be seen, signals of tone burst and sine wave cases are in almost perfect agreement. Whilst this argument has focused on the effect of misalignment in reception when trying to select between symmetric or antisymmetric modes, the same analysis holds for misalignment on dual transmission.

C. Experimental setup

Experiments were performed using a RITEC® RPR-4000 Pulser/Receiver to generate and receive the signals from the EMATs. The excitation pulse was set to an 8 cycle tone burst at 311 kHz and 367 kHz to generate SH0 and SH1 modes, respectively, as in the simulation. After passing through the internal amplifier the received signal was acquired by an oscilloscope, with the driver and oscilloscope being connected to a PC to automate data capture. Both transmitter and receiver EMATs were 3 cycle, 10 mm nominal wavelength PPM EMATs from Sonemat Ltd. The test sample was an 8 mm thick, 800 mm long and 250 mm wide aluminium plate. The plate length was chosen in order to ensure that echoes reflected from the plate's end would not interfere with the waves of interest; the width of the plate was chosen to ensure that no guided waves that were reflected from the edge of the plate would interfere with the waves of interest.

To ensure that EMATs on both surfaces are well aligned, a holder frame was built, as shown in Fig. 10. The plate was vertically located into a slot to fit the its thickness. The position of the plate relative to the frame was constrained by fastening screws. The positions of the EMATs are predefined by pairs of plastic brackets; both brackets of each pair are in exact the same position but on both sides of holder. The EMATs were placed in the brackets and fastened against the plate's surface by screws. Provided that the bottom and rear faces of the EMATs were well positioned against the lower and rear walls of the brackets, their position was sufficiently accurate and consistent.

In order to verify the effectiveness of the supporting frame and the accurate positioning of the EMAT on both surfaces, a non defective aluminium plate was initially used. In this case only the signals given by (10a) and (10d) should be non-zero, as there is no mechanism for mode conversion. Signals from (10b) and (10c) were then calculated and its value compared to (10a) and (10d) in order to assess the mode separation capability.

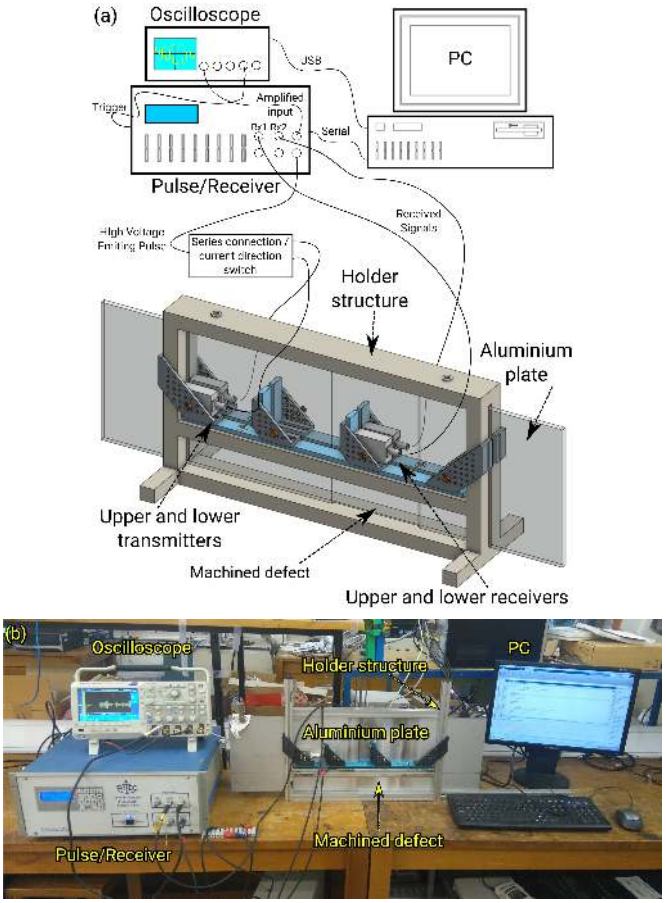

Fig. 10. Experimental setup with holder frame structure. Schematic (a) and photograph (b).

Fig. 11(a) and (b) show experimental signals obtained by the superposition principle at x=405 mm, for symmetric (at 311 kHz) and antisymmetric (at 367 kHz) generation in order to generate only the SH0 and SH1 modes, respectively. The reception in the same polarisation of transmission, calculated through (10a) and (10d), as well as in the opposite polarisation, (10b) and (10c), are shown black and grey lines, respectively. The grey line should ideally be zero as there should be no mode conversion in a defect free plate. As it can be seen the grey lines show very low amplitude. The raw signals for transmitter and receiver at the top and bottom surfaces of the plate are shown in the inset plots. The top (resp. bottom) inset plot is centred at an instant where SH0 (resp. SH1) predominates over SH1 (resp. SH0). In the top plot one can see that all components are in phase, whereas in the bottom plot the components received at the top and bottom surfaces are out of phase. This agrees with the modes' symmetry characteristics and allows separation as seen in the full plot.

The ratio of the peak-to-peak amplitude of signals (10b) to (10a) or (10c) to (10d), can be used to quantitatively assess

TABLE I
OPPOSITE TO SAME POLARISATION PEAK-TO-PEAK RATIO FOR SH0 AND SH1 GENERATED IN A NON DEFECTIVE PLATE.

	Superposition principle		Dual excitation	
	SH0 (%)	SH1 (%)	SH0 (%)	SH1 (%)
receiver position (mm)	$\frac{p\text{-}p\{u_A\|_S\}}{p\text{-}p\{u_S\|_S\}}$	$\frac{p\text{-}p\{u_S\|_A\}}{p\text{-}p\{u_A\|_A\}}$	$\frac{p\text{-}p\{u_A\|_S\}}{p\text{-}p\{u_S\|_S\}}$	$\frac{p\text{-}p\{u_S\|_A\}}{p\text{-}p\{u_A\|_A\}}$
113	6.22	2.51	16.47	4.43
257	6.27	6.24	11.35	5.74
405	2.23	1.82	4.72	2.09

the effectiveness of the mode separation procedure, with a lower value indicating a more effective mode separation. This calculation is shown in the second and third columns of Table I for three sensing positions.

Generation by dual excitation was achieved using two nominally identical EMATs, connected in series with the current direction in one EMAT injected in two different directions to provide a purely symmetric and purely antisymmetric generation source. The detection was done differently, by repositioning the same EMAT receiver on either side of the plate and acquiring a new signal. These signals are shown in Fig. 11(c) and (d) for the SH0 and SH1 modes, respectively, and are very similar to those calculated by the superposition principle [Fig. 11(a) and (b)], confirming the validity of superposition procedure. The grey lines are, however, larger amplitude, suggesting that using two different EMAT transmitters has yielded a large difference on the induced forces on both surfaces, which would generate a less pure symmetric or antisymmetric mode. This is confirmed by observing the raw signals in the bottom inset plot of Fig. 11(c) and in the top inset plot of Fig. 11(d) which should be ideally zero, since a symmetric, resp. antisymmetric, generation was performed. The ratio of the opposite to the same polarisation amplitude for this case is shown in the fourth and fifth columns of Table I, and has higher values, confirming a less effective mode selection.

D. Mode conversion analysis

After validating the mode selectivity technique, mode conversion was experimentally quantified in a plate with a region that had been machined thinner, to a depth of 5 mm, as in the simulation. The superposition principle was used hereinafter, since it was deemed more accurate in the defect-free plate analysis. Mode conversion was investigated reflected from the edge of the machined region (detected at 113 mm, 69 mm before the machined edge), passing through the thinner region (at 257 mm, on the middle of the machined region) and transmitted out of the far edge of the thinner region into the thicker, unmachined, region of the plate (received at 405 mm, 73 mm, after the end of the thinner region). Experimental signals and FE simulations were compared, normalizing the simulated signal amplitude, so that the amplitude of the incident wave mode matched experimental signals at each position.

Fig. 12 shows the signals detected at the three positions when SH0 mode is generated at 311 kHz. The continuous and the dashed rectangles represent the theoretical expected arrival time gates for direct and reflected waves, respectively, calculated considering the different group velocity along the propagating path, due to mode conversion, and the pulse duration. Fig. 12(a) shows the symmetric generation with symmetric reception. Reflected echoes in the experimental data have lower amplitude than in the simulated data, because attenuation was not included in the numerical model. The SH0 wave that has been mode converted to an SH1 mode due to reflection at the machined edge is shown in Fig. 12(b). Fig. 12(c) and (d) show the symmetric and antisymmetric reception on the middle of the defect. As the remaining thickness is below the cut-off thickness of the SH1 mode, no antisymmetric wave mode should propagate inside the defect. Observing Fig. 12(d) one can see that the simulated signal indeed show a constant zero value, whereas a low amplitude oscillation is seen for the experimental signal; this is an experimental artefact due to misalignment, as assessed in section VI-B [similar imprecision can be found in Fig.13(c) and at about 50 μs in Figs.12(b) and 13(b)]. A low amount of the transmitted symmetric SH0 mode is reflected at the defect's right end, seen in the dashed rectangle of Fig. 12(c), whilst most of its energy is transmitted out of the defect, split between SH0 and SH1 modes, Fig. 12(e) and (f), respectively.

The same analysis can be drawn for the generated SH1 at 367 kHz, shown in Fig. 13. In this case any wave detected on the thinner region is due to mode conversion to SH0 [Fig. 13(d)] since the original mode cannot propagate in such a thin region, as verified in Fig. 13(c). Despite no antisymmetric SH mode being present inside the machined region, one is generated at the far edge of the machined region, arising from the SH0 modes within the thinner region mode converting to SH1 when leaving the thinner region. This mechanism can arise when either an SH0 or SH1 mode is incident on the thinner region.

All wave modes arrived in the expected time gates, represented by rectangles in Figs.12 and 13, confirming that the mode selectivity technique is indeed effective in identifying mode conversion. In the case when the SH0 mode is generated, the mode-converted wave arrives latter in time than the original mode, due to the lower group velocity of the SH1 mode. When the SH1 mode is generated, the opposite happens. However the time difference is not enough to allow the modes to be distinguished in time. This can be seen by observing the signal inside the dashed (a) an (b) and continuous rectangles (e) and (f) in Fig. 12 and 13. Observing Figs.12 and 13, one can see that simulation and experimental data show very good agreement. The non-mode converted modes, (a), (c) and (e), present a higher level of similarity than mode converted signals, (b), (d) and (f). One reason for this is the fact that the effect of the transducer misalignment on both surfaces is less severe when computing the signals from waves that have not been generated by mode conversion, according to (15). Another reason for this is that there is a wavelength shift when mode conversion occurs, which due to the nature of the PPM EMAT causes signal distortion, since mode's wavelength moves away from the peak response of the transducer's spatial bandwidth. There has been an attempt to include this effect in the numerical data in Fig. 12 and 13 by performing a

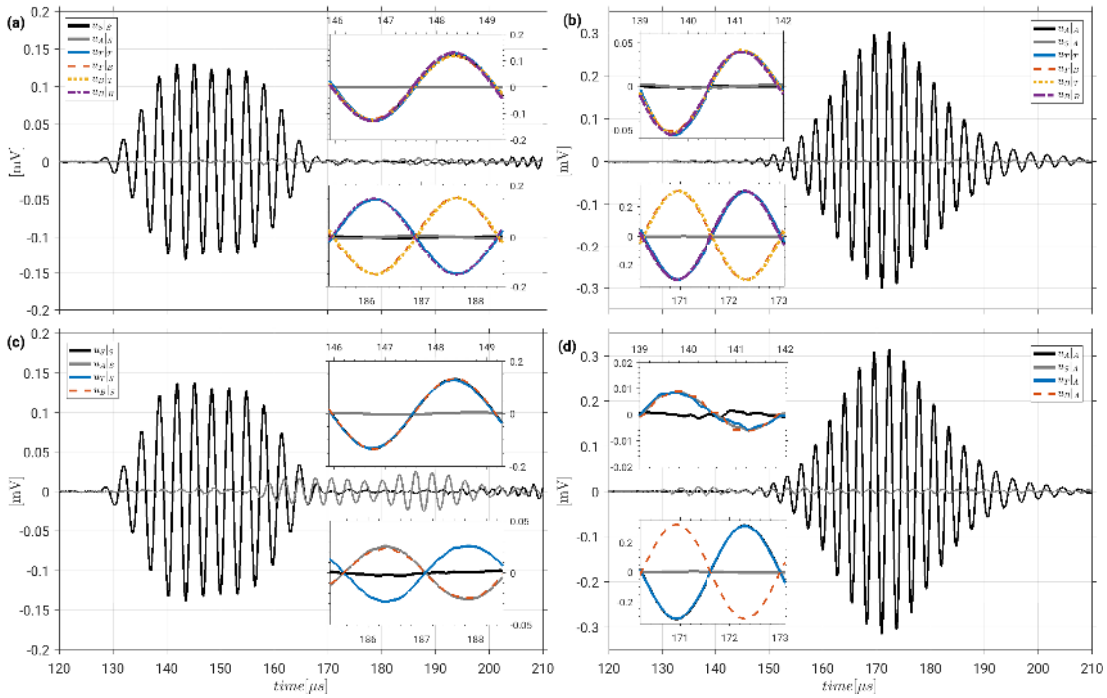

Fig. 11. Mode separation by superposition principle (a and b) and dual excitation (c and d) at a defect free plate received at 405mm. SH0 generated at 311 kHz (a and c) and SH1 generated at 367 kHz (b and d). Black (resp. grey) line represents reception at same (resp. opposite) polarisation as transmission. Insets show raw signals in time intervals where SH0 predominate (top insets) and SH1 predominate (bottom insets).

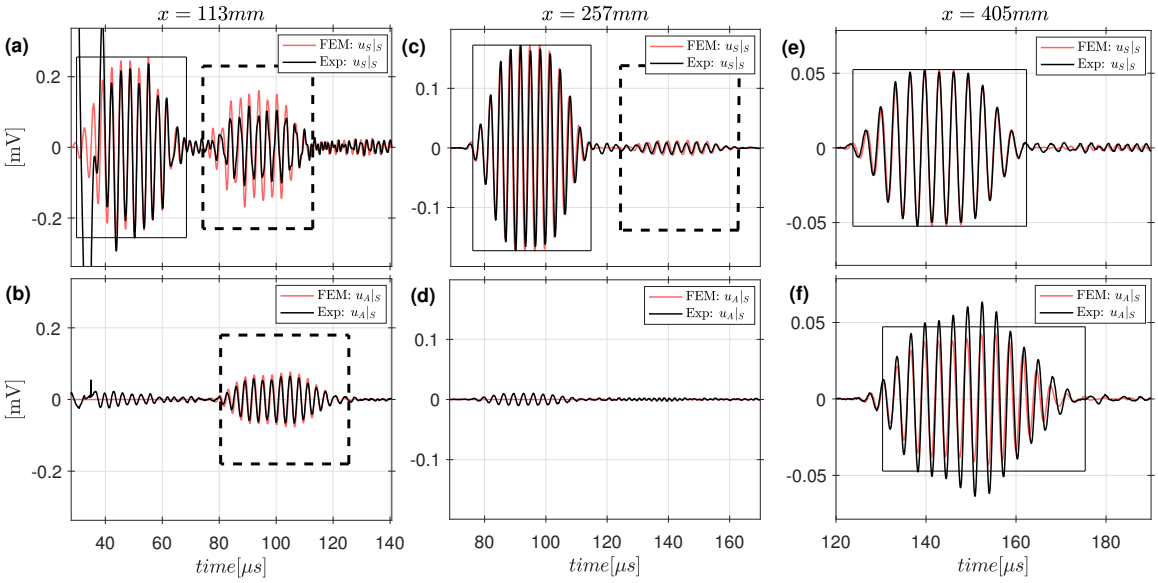

Fig. 12. Experimental (black) and simulation (red) signals for SH0 generated at 311 kHz in a plate with defect received before the defect (a and b), on the defect (c and d) and after the defect (e and f). Continuous rectangles represent the theoretical arrival times of the direct waves and dashed rectangle of the waves reflected at defect ends. Non-mode converted signals (a, c and e), mode converted signals (b, d and f).

spatial convolution with the EMATs spatial profile, which was approximated by spatial tone burst.

In order to further illustrate the strength of the technique Fig. 14 shows how the signal would look if the conventional pitch catch method was used with both transmitter and receiver placed on the face opposite to where the thinner region was machined, attempting to generate the SH0 mode by setting the frequency at 311 kHz with receiver after the end of the region. Comparing Fig. 14 with Figs.12(e) and (f) one can see that the presence of both modes are mixed in the raw signal, making any mode identification impossible. The non-pure generation of the SH0 mode due the operating region of the EMAT (see Fig. 2.(b)) and mode conversion contribute to the received signal shape.

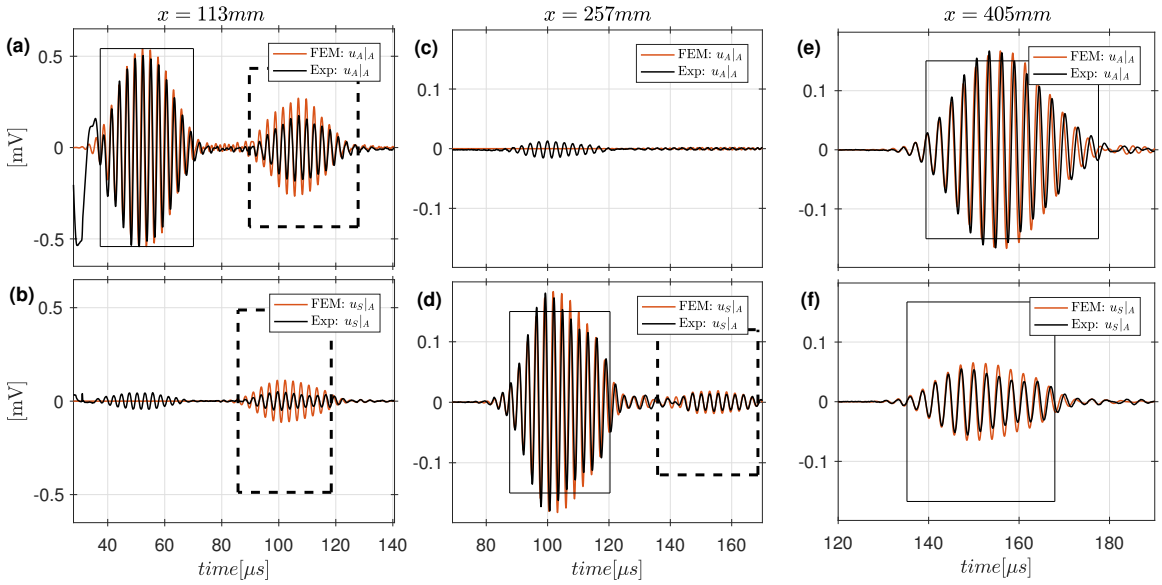

Fig. 13. Experimental (black) and simulation (red) signals for SH1 generated at 367 kHz in a plate with defect received before the defect (a and b), on the defect (c and d) and after the defect (e and f). Continuous rectangles represent the theoretical arrival times of the direct waves and dashed rectangle of the waves reflected at defect ends. Non-mode converted signals (a, c and e), mode converted signals (b, d and f).

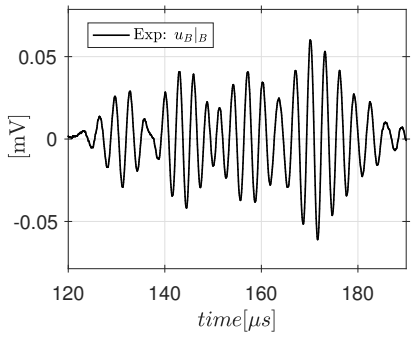

Fig. 14. Experimental signals received at 405 mm, both transmitter and receiver were placed on the bottom surface, generation at 311 kHz.

VII. Conclusions

Combining dual excitation and dual reception of SH guided waves modes with PPM EMATs was validated as an experimental methodology for mode selection and mode conversion analysis. Dual transmission on both surfaces of the plate ensures single mode generation, even if the temporal and spatial pulse bandwidths encompass two modes of opposing symmetry. A similar procedure was employed in reception in order to separate symmetric from antisymmetric modes that have originated from mode conversion. The technique's vulnerability to EMAT misalignment was theoretically modelled by a simple continuous wave model and confirmed by numerical simulation of tone burst wave. The error due to misalignment on the selection of a wave arising from mode conversion is considerably greater than when selecting a mode that has not arisen due to mode conversion.

The technique can be implemented in two versions, by connecting two PPM EMAT transducers in series, or by using the superposition principle. Provided that access to both surfaces of the plate is granted, the two main experimental issues affect the technique, namely how identical the EMATs are and the degree of misalignment between EMAT positions on both surfaces. Experimental evaluation of the proposed methodology in a specially designed structure to ensure alignment, revealed that the superposition version is preferred, presenting less than about 6% error, against less than about 16% for the dual excitation version for the EMATs that were available. Nevertheless, the use of the superposition principle is more time consuming since twice as many readings are required.

The procedure was verified for a plate with a machined thinner region in which SH modes undergo mode conversion when interacting with it, and due to the plate's length, separation in time was not possible. Experimental and numerical results are in very good agreement, validating the adopted finite element model for SH waves interacting with wall thinning. The expected arrival times of mode converted and non-mode converted SH modes, as well as the absence significant antisymmetric signals on the machined region that left a thickness of aluminium thinner than the SH1 cut-off thickness, proved the effectiveness of the technique in selecting symmetric and antisymmetric modes. The case studied here confirmed some of the qualitative conclusions of previous works [8], [9], such as the observation that the SH1 mode incident on a thin region of plate mode converts to SH0 inside deep defect and is then converted back to an SH1 mode on exiting the thinner plate region.

In realistic situations having access to both surfaces of a sample is unlikely, and sufficiently precise positioning of transducers would be extremely difficult even if both side of the sample could be accessed. However, the technique described in this paper is not intended to propose a realistic testing geometry, but rather provides insight and a methodology for quantitative mode conversion analysis and a deeper

understanding of the interaction of SH guided waves with simulated defects through quantitative numerical modelling and experimental validation. Reliable mode conversion analyses have meaningful practical relevance for further establishing a final inspection procedure, such as one relying on conventional single side application. For instance, the method presented in this paper overcomes the limitation in obtaining quantitative data of mode conversion [6]–[9], allowing both modes to be completely separated for further analysis. Coefficients for transmission and reflection to the defect could be experimentally calculated, for arbitrary defect shape profiles, which are necessary for further interpreting data of real defects in practical inspections. The proposed technique has also potential for similar analysis in other types of guided waves, such as Lamb waves.

ACKNOWLEDGEMENTS

Authors would like to thank the Brazilian National Council for Scientific and Technological Development, CNPq, for financial support.

REFERENCES

[1] M. Hirao and H. Ogi, *EMATs for science and industry: noncontacting ultrasonic measurements*. Springer Netherlands, 2003.

[2] M. G. Silk, *Ultrasonic transducers for nondestructive testing*. Bristol: Hilger, 1984.

[3] P. A. Petcher and S. Dixon, "Weld defect detection using PPM EMAT generated shear horizontal ultrasound," vol. 74, pp. 58–65, 2015.

[4] R. Ribichini, F. Cegla, P. B. Nagy, and P. Cawley, "Study and comparison of different EMAT configurations for SH wave inspection," *IEEE Transactions on Ultrasonics, Ferroelectrics, and Frequency Control*, vol. 58, no. 12, pp. 2571–2581, December 2011.

[5] X. Zhao and J. L. Rose, "Guided circumferential shear horizontal waves in an isotropic hollow cylinder," *The Journal of the Acoustical Society of America*, vol. 115, no. 5, pp. 1912–1916, 2004.

[6] M. Clough, M. Fleming, and S. Dixon, "Circumferential guided wave EMAT system for pipeline screening using shear horizontal ultrasound," *NDT and E International*, vol. 86, pp. 20 – 27, 2017.

[7] M. Hirao and H. Ogi, "An SH-wave EMAT technique for gas pipeline inspection," *NDT & E International*, vol. 32, no. 3, pp. 127 – 132, 1999.

[8] Nurmalia, N. Nakamura, H. Ogi, and M. Hirao, "Detection of shear horizontal guided waves propagating in aluminum plate with thinning region," *Japanese Journal of Applied Physics*, vol. 50, no. 7S, p. 07HC17, 2011.

[9] Nurmalia, N. Nakamura, H. Ogi, M. Hirao, and K. Nakahata, "Mode conversion behavior of SH guided wave in a tapered plate," *NDT & E International*, vol. 45, no. 1, pp. 156 – 161, 2012.

[10] P. A. Petcher and S. Dixon, "Mode mixing in shear horizontal ultrasonic guided waves," *Nondestructive Testing and Evaluation*, pp. 1–20, 2016.

[11] P. Hora and P. Cervena, "Determination of lamb wave dispersion curves by means of fourier transform," *Applied and Computational Mechanics*, vol. 6, pp. 5–16, 2012.

[12] D. Alleyne and P. Cawley, "A two-dimensional fourier transform method for the measurement of propagating multimode signals," *The Journal of the Acoustical Society of America*, vol. 89, no. 3, pp. 1159–1168, 1991.

[13] M. Niethammer, L. J. Jacobs, J. Qu, and J. Jarzynski, "Time-frequency representations of lamb waves," *The Journal of the Acoustical Society of America*, vol. 109, no. 5, pp. 1841–1847, 2001.

[14] S. Wang, S. Huang, Q. Wang, Y. Zhang, and W. Zhao, "Mode identification of broadband lamb wave signal with squeezed wavelet transform," *Applied Acoustics*, vol. 125, pp. 91 – 101, 2017.

[15] W. H. Prosser, M. D. Seale, and B. T. Smith, "Time-frequency analysis of the dispersion of lamb modes," *The Journal of the Acoustical Society of America*, vol. 105, no. 5, pp. 2669–2676, 1999.

[16] T. Yamasaki, S. Tamai, and M. Hirao, "Optimum excitation signal for long-range inspection of steel wires by longitudinal waves," *NDT & E International*, vol. 34, no. 3, pp. 207–212, 2001.

[17] K. Xu, D. Ta, P. Moilanen, and W. Wang, "Mode separation of lamb waves based on dispersion compensation method," *The Journal of the Acoustical Society of America*, vol. 131, no. 4, pp. 2714–2722, 2012.

[18] D. Schmidt, M. Sinapius, and P. Wierach, "Design of mode selective actuators for lamb wave excitation in composite plates," *CEAS Aeronautical Journal*, vol. Vol. 3, pp. 1–8, January 2013.

[19] D. Schmidt, P. Wierach, and M. Sinapius, "Mode selective actuator-sensor system for lamb wave-based structural health monitoring," in *7th European Workshop on Structural Health Monitoring*, 2014, Conference Proceedings, pp. 325–332.

[20] J. P. Koduru and J. L. Rose, "Mode controlled guided wave tomography using annular array transducers for shm of water loaded plate like structures," *Smart Materials and Structures*, vol. 22, no. 12, p. 125021, 2013.

[21] P. Y. Moghadam, N. Quaegebeur, and P. Masson, "Mode selective generation of guided waves by systematic optimization of the interfacial shear stress profile," *Smart Materials and Structures*, vol. 24, no. 1, p. 015003, 2015.

[22] ——, "Design and optimization of a multi-element piezoelectric transducer for mode-selective generation of guided waves," *Smart Materials and Structures*, vol. 25, no. 7, p. 075037, 2016.

[23] Z. Su and L. Ye, "Selective generation of lamb wave modes and their propagation characteristics in defective composite laminates," *Proceedings of the Institution of Mechanical Engineers, Part L: Journal of Materials: Design and Applications*, vol. 218, no. 2, pp. 95–110, 2004.

[24] Y.-H. Kim, D.-H. Kim, J.-H. Han, and C.-G. Kim, "Damage assessment in layered composites using spectral analysis and lamb wave," *Composites Part B*, vol. 38, no. 7-8, pp. 800–809, 2007.

[25] A. Shelke, T. Kundu, U. Amjad, K. Hahn, and W. Grill, "Mode-selective excitation and detection of ultrasonic guided waves for delamination detection in laminated aluminum plates," *IEEE Transactions on Ultrasonics, Ferroelectrics, and Frequency Control*, vol. 58, no. 3, pp. 567–577, March 2011.

[26] S. Liu, Y. Zhang, C. Zhang, and Q. Yang, "Finite element analysis for the inhibition of electromagnetic acoustic testing (EMAT) Lamb waves multi-modes," in *43rd Review of Progress in Quantitative Nondestructive Evaluation*, ser. American Institute of Physics Conference Series, vol. 1806, Feb. 2017, p. 050014.

[27] S. Dixon, P. A. Petcher, Y. Fan, D. Maisey, and P. Nickolds, "Ultrasonic metal sheet thickness measurement without prior wave speed calibration," *Journal of Physics D: Applied Physics*, vol. 46, no. 44, p. 445502, 2013.

[28] J. L. Rose, *Ultrasonic Guided waves in solid media*. Cambridge University Press, 2014.

[29] P. Petcher, S. Burrows, and S. Dixon, "Shear horizontal (sh) ultrasound wave propagation around smooth corners," *Ultrasonics*, vol. 54, no. 4, pp. 997 – 1004, 2014. [Online]. Available: http://www.sciencedirect.com/science/article/pii/S0041624X13003351